Photokinetic Analysis of PRODAN and LAURDAN in Large Unilamellar Vesicles from Multivariate Frequency-Domain Fluorescence

Brad A. Rowe and Sharon L. Neal*

Department of Chemistry & Biochemistry, University of Delaware, Newark, Delaware 19716

Received: September 6, 2003; In Final Form: November 17, 2004

This paper describes a multivariate photokinetic analysis of the membrane phase dependence of PRODAN and LAURDAN photokinetics in DMPC vesicles. Decay data, arranged in the form of Fourier transformed emission-decay matrices (FT-EDMs), were collected as a function of temperature around the gel phase transition temperature. Each matrix was partitioned into the emission spectra and decay profiles of the underlying emission components using methods based on principal components analysis. The analysis revealed that both probes typically emit at least three spectral components, which vary in intensity as the membrane undergoes gel to liquid-crystalline phase transitions: a locally excited species ($\lambda_{max} \sim 415$ nm), a charge-transfer species ($\lambda_{max} \sim 435$ nm), and a solvent relaxed species ($\lambda_{max} \sim 490$ nm). In contrast to previous reports, the most red-shifted species is not photoexcited, but evolves from the locally excited species and does not exhibit the dynamic Stokes' shifts associated with conventional solvent relaxation. The primary difference in the emission of the two probes is the prominence of the charge-transfer species in the LAURDAN emission.

Introduction

Phospholipid membranes constitute the basic framework of cell walls and form assemblies that house proteins and enzymes whose activities are critical to the execution of cell processes. The phase state of a membrane can be particularly relevant to the function of these membrane proteins.[1−4] Membrane phase state can be affected by many factors including temperature, pressure, lipid composition, and the presence of other molecules embedded in the membrane matrix. The heterogeneity of constituents in many natural membranes can lead to coexisting phase domains.[5,6] Therefore, there is a need to characterize lipid membranes with sufficient selectivity to detect variations around bulk properties. One method that can provide this level of selectivity utilizes multi-emissive state fluorescent probes to detect the heterogeneity of lipid membranes. Multi-emissive state fluorescent probes have emission profiles that change, typically as a result of excited-state processes, depending on microenvironment.[7−11] While the spectral responses of these types of probes have been useful for generating information about probe microenvironments, unambiguous microenvironment characterization is difficult. This paper investigates the combined spectral and dynamic response of classic multi-emissive state fluorescent probes to phase changes in large unilamellar vesicles and examines the correlation between the subpopulations of excited probes detected and probe microenvironments.

Two multi-emissive state probes that have been widely used in membrane studies are 6-propionyl-2-dimethylaminonaphthalene (PRODAN), first designed and synthesized in the group of Gregorio Weber in 1979,[12] and a fatty acid derivative, 6-dodecanoyl-2-dimethylaminonaphthalene (LAURDAN) (see Figure 1 for structures). Originally developed to study dipolar relaxation, these probes' sensitivity to local polarity and phase in lipid membranes has found use in a variety of studies, including investigations of interfacial properties of ether lipids,[13,14] alcohol interactions with biological membranes,[15] surface properties of cholesterol containing membranes,[16,17] water content of reverse micelles,[18] polarity and packing of lipid bilayers,[19] structure of interdigitated bilayers,[20] thermotropic properties of phosphotidylethanols,[21] and oxidative damage of phospholipids.[22] One of the most widely reported applications of PRODAN and LAURDAN in lipid research is the study of membrane phase. The emission spectra of PRODAN and LAURDAN exhibit dramatic red shifts in lipid membranes subjected to gel to liquid-crystalline phase transitions. These shifts have been attributed to solvent relaxation of excited-state molecules in liquid-crystalline phases of the membrane. Thus, the two most prominent spectral bands, blue (~435 nm) and green (~490 nm), usually are attributed to the emission of probes in the gel and liquid-crystalline membrane phases, respectively. There are two prevailing hypotheses regarding the source of this spectral shift in membranes. In the first, the shift reflects differences in the positions and orientations of probe molecules at the hydrophilic−hydrophobic interface of membranes.[23,24] Chong and co-workers concluded that the polarity of these local environments dictates the extent of solvent

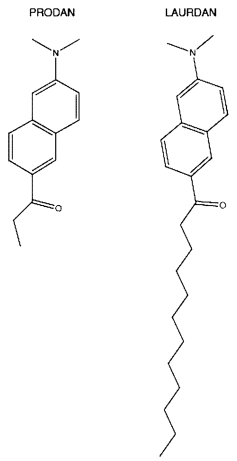

Figure 1. Structures of PRODAN and LAURDAN.

* Corresponding author. E-mail: sneal@udel.edu.

10.1021/jp036664n CCC: $33.50
Published on Web 07/07/2006

relaxation from their studies at high pressure and their work with interdigitated lipids. In the second hypothesis, the position of the probe molecules (at least in the case of LAURDAN) is thought to be constant, with variations in the structure and interactions of surrounding lipid and water molecules producing differences in the extent of solvent relaxation.[25]

The nature and origin of the shift in the PRODAN spectrum in isotropic solvents has been studied extensively. The details of PRODAN excited-state photokinetics are complex and the interpretation of experimental results has been debated. Weber and Farris first correlated PRODAN spectral shifts to dipolar relaxation in response to solvent polarity.[12] They concluded that a substantial change in dipole moment upon excitation accounts for the large Stokes' shift in polar media. Evidence that continuous solvent relaxation does not play a role in PRODAN photokinetics came from Lakowicz and Balter, who were able to resolve two spectral components from phase-modulation fluorescence measurements of PRODAN in *n*-butanol.[26] They also demonstrated that PRODAN solvent relaxation in *n*-butanol proceeds in at least two steps, with a possible intermediate. On the other hand, Chapman and co-workers published time-resolved results that suggested continuous solvation of PRODAN—evidence against an activated charge-transfer process.[27,28] Most recently, Abelt and coworkers have synthesized PRODAN derivatives in which the orientation of the dialkylamino group is fixed relative to the aromatic rings.[29,30] Their results indicate that fixing the amine nitrogen so that the lone pair cannot be conjugated to the ring system substantially changes the chromophore's spectral profile and reduces its quantum yield, establishing the role of charge transfer in PRODAN emission.

Debate also arose around the results of the theoretical studies that have been conducted. Many investigators agree that the ground state of PRODAN is planar,[31,32] but the conformation of the excited state and origin of the Stokes' shift in polar media has been debated. Several semiempirical calculations,[31−35] supported by time-dependent fluorescence measurements,[36] indicate that the Stokes' shift arises from a twisted intramolecular charge transfer (TICT) state stabilized by solvent interactions. However, Ilich and Prendergast contended that a naphthalene ring deformation accompanies the twisted intramolecular charge transfer[32] and comparison of the properties e.g., emission maxima and apparent excited state dipole moment, of PRODAN and a known TICT probe generated little support for the existence of a TICT for PRODAN.[37] Parusel and coworkers laid the foundation for the resolution of this inconsistency: they noted the dependence of the geometry of the lowest energy state on the choice of the Onsager radius. Increasing the Onsager radius (lowering the apparent solvent polarity) indicated that Stokes' shifted emission occurs from a PICT state (planar ICT)[35] as was later observed in geometrically constrained derivatives.[29]

In the late 1980s and early 1990s, the focus began to shift from conformation to excited-state/solvent interactions. Balter and co-workers disputed the extent of the change in dipole moment upon excitation originally calculated for PRODAN and suggested that solvent-specific interactions may play a role in the large Stoke's shift observed in protic solvents.[38] Furthermore, Catalan and co-workers pointed out that regression analyses comparing PRODAN emission maxima in a wide range of solvents show weak correlation between solvent polarity and Stokes' shift, particularly in protic solvents, then called the invocation of a TICT state into question.[39] In their view, solvent−solute interactions, specifically solvent acidity and basicity, are adequate to describe the large Stokes' shift. Other researchers have come to similar conclusions when comparing the Stokes' shift in protic and aprotic solvents.[15,40] Finally, transient dielectric loss measurements determined the change in the dipole moment upon excitation of PRODAN to be 4.4−5 D, which is far less than previously reported values determined using indirect methods.[41] These results suggest that a charge transfer state is insufficient to describe the large Stokes' shift observed in polar solvents, and that specific solvent interactions such as hydrogen bonding play crucial roles in PRODAN emission.

The studies of PRODAN photokinetics described in the previous paragraphs were conducted in simple solvents. In these systems, it is reasonable to think of excited state molecules undergoing one type of solvent interaction or another. However, the most widely used application of these probes is in lipid membrane studies, where excited molecules can be exposed to several different local environments. In these environments, it is possible, if not probable, that the excited-state probes undergo more than one type of solvent interaction. Most membrane studies utilizing these probes analyze their spectra as combinations of two phase dependent (gel and liquid-crystal) components,[15−17,19,21,25,42−52] with the decay kinetic analysis playing a secondary role. This approach does not account for underlying excited-state processes. However, there is evidence of more than two emission states, even in homogeneous phases of lipid membranes. In gel phase DPPC vesicles, Lakowicz and coworkers recorded a small red shift in the time-resolved emission spectra (TRES) of PATMAN (PRODAN derivative with palmitoyl substituted for the prolyl chain) along with a much larger shift after the phase transition.[53] In time-dependent fluorescence studies of LAURDAN in vesicles,[54] viscous oils, and frozen ethanol,[55] Paternostre and co-workers found evidence of three emitting states. Fishov and co-workers recovered three spectral components from LAURDAN in *E. coli* membranes at 11 °C and 37 °C.[56]

Complete characterization of PRODAN and LAURDAN photokinetics in lipid membranes is a prerequisite to membrane phase characterization based on correlations between local probe environment and excited-state interactions. In pursuit of this goal, this paper describes a multivariate analysis of the phase dependence of PRODAN and LAURDAN photokinetics in lipid membranes conducted to investigate the details of the interactions of the probes' excited states. After measuring decay profiles at multiple wavelengths, the data were arranged in the Fourier transformed emission-decay matrix (FT-EDM) format. Data in this format can be partitioned into sets of component spectral and decay responses using minimal photokinetic model assumptions by multivariate data analysis methods based on principal components analysis.[57−59] Moreover, nonheuristic, statistical methods for determining the number of components contributing to matrix formatted data (rank estimation) are available.[60,61] The Fourier transformed emission-decay matrices of the probes' emission in DMPC vesicles were measured as a function of temperature around the DMPC gel phase transition temperature. Analysis of the matrices revealed that both probes typically emit at least three spectral components, which vary in intensity as the membrane undergoes gel to liquid-crystalline phase transitions. The spectral components are assigned to locally excited, charge transfer, and solvent relaxed species, a modification of the assignments used by Paternostre et al.[55] The multivariate analysis indicated that the most red-shifted species is not photoexcited, but formed via excited-state reaction. In contrast to the results of Paternostre et al., this species appears

to be generated from the locally excited state rather than the charge transfer state and does not exhibit the dynamic Stokes' shifts typically associated with solvent relaxation. The principal difference observed in the emission of the two probes is the greater emission intensity of the charge-transfer component of LAURDAN.

Materials and Methods

Fluorescence Instrumentation. Fourier transformed emission-decay matrices (FT-EDMs) were measured using a lifetime spectrofluorometer (K2, ISS, Champaign, IL). The samples were excited at 368 nm using the output of a frequency-tripled, cavity-dumped, mode-locked Ti:sapphire laser (Mira 900-F, Coherent, Santa Clara, CA) pumped by a 10 W Nd:YVO_4 frequency-doubled laser (Millenia X, Spectra-Physics, Mountain View, CA). A Soliel-Babinet compensator (RC-10, Optics for Research, Caldwell, NJ) fixed the polarization of the excitation beam to vertical. The fluorescence was collected 90° to the excitation, through a polarizer set to 54.7° from the vertical (magic angle) and a 390 nm long-pass filter. The emission decay profiles at several wavelengths, selected by a monochromator, were collected on a photomultiplier tube (type R928, Hamamatsu). Fluorescence spectra were corrected using a standard quinine sulfate dihydrate solution in 0.5 M H_2SO_4. The temperature of the sample was held constant in a water-jacketed fluorescence cell connected to a temperature controlled water bath (Isotemp refrigerated circulator model 910, Fisher Scientific). Temperature inside the fluorescence cell was monitored by a digital thermometer (model 63-1032, Radio Shack) immediately before data acquisition.

Sample Preparation. 6-Propionyl-2-dimethylaminonaphthalene (PRODAN) and 6-dodecanoyl-2-dimethylaminonaphthalene (LAURDAN) were used as received from Molecular Probes (Eugene, OR). Stock solutions were prepared in HPLC-grade ethanol (200 proof, Pharmco, Brookfield, CT). 1,2-Dimyristoyl-s*n*-glycero-3-phosphocholine (DMPC) was purchased in powdered form and used as received from Avanti Polar Lipids (Alabaster, AL). The appropriate amount of DMPC to yield 1 mM lipid solutions and the probes were transferred in ethanol to a glass vial and air-jet dried overnight. The dried probe/lipid mixture was then suspended in a buffer solution of 0.01 M $NaPO_4$, pH 6.6 in HPLC-grade water (Alfa Aesar, Ward Hill, MA) and sonicated for at least 1 hour. Large unilamellar vesicles were formed by extrusion through 0.1 μm pore membranes (Extruder, Avanti Polar Lipids, Alabaster, AL) a minimum of 15 times. All sample solutions were prepared fresh daily and used immediately. All solvents exhibited negligible background fluorescence.

Data Analysis. *Data Structure.* When the decay of a mixture of fluorophores is measured as a function of emission wavelength, the decays can be arranged to form an emission-decay matrix (EDM). Each matrix row is the decay measured at a different wavelength. In frequency domain matrices, each column is the sum of the components of the oscillating emission that are in (real) and out (imaginary) of phase with the excitation at a different modulation frequency. This format is an alternative to representing multiple wavelength frequency-domain decay data as phase shifts and demodulation factors that preserves the linearity of the fluorescence response. In other words, the FT-EDM of an N component mixture is the sum of the FT-EDMs of the individual components, i.e.,

$$\tilde{\mathbf{D}} = \sum_{n=1}^{N} \tilde{\mathbf{D}}_n = \sum_{n} \mathbf{x}_{\bullet n}\tilde{\mathbf{y}}_{\bullet n}^{\mathrm{T}} = \mathbf{X}\tilde{\mathbf{Y}}^{\mathrm{T}} \tag{1}$$

where, $\tilde{\mathbf{D}}_n$, $\mathbf{x}_{\bullet n}$, and $\tilde{\mathbf{y}}_{\bullet n}$ are the matrix, emission spectrum, and FT decay of the nth component, respectively. In most cases, the pure FT decays of the mixture components, $\tilde{\mathbf{Y}}$, are solutions of a system of coupled first-order differential equations, i.e.,

$$\frac{d\mathbf{y}^{\mathrm{T}}}{dt} = \frac{d}{dt}\begin{bmatrix} y_1 \\ \vdots \\ y_N \end{bmatrix} = \begin{bmatrix} -k_{11} & \cdots & k_{1N} \\ \vdots & \ddots & \vdots \\ k_{N1} & \cdots & -k_{NN} \end{bmatrix}\begin{bmatrix} y_1 \\ \vdots \\ y_N \end{bmatrix} + \begin{bmatrix} f(t) \\ \vdots \\ f(t) \end{bmatrix} = \mathbf{K}\mathbf{y}^{\mathrm{T}} + \mathrm{f}(t)\mathbf{j}. \tag{2}$$

where the $N \times N$ photokinetic transfer matrix, $\mathbf{K}$, consists of the decay rates of all the excited-state species in the sample (on the diagonal) and the rates of the interactions between the excited-state species (on the off-diagonals). When the excitation function, $f(t)$ in eq 2, is harmonic, the emission components oscillate at the same frequency as the excitation, but the fraction of each component that is in or out of phase with the excitation is different, reflecting the rates of the relaxation processes affecting that species. Generally, these oscillating signals are measured at several, M, modulation frequencies. The frequency domain decays of the N components can be collected on the columns the $M \times N$ matrix $\tilde{\mathbf{Y}}$, which is

$$\tilde{\mathbf{Y}} = \left(\frac{1}{\Delta t}\right)\begin{bmatrix} (\lambda_1 - i\omega_1)^{-1} & \cdots & (\lambda_N - i\omega_1)^{-1} \\ \vdots & \ddots & \vdots \\ (\lambda_1 - i\omega_M)^{-1} & \cdots & (\lambda_N - i\omega_M)^{-1} \end{bmatrix}\begin{bmatrix} \gamma_1 & 0 & 0 \\ 0 & \ddots & 0 \\ 0 & 0 & \gamma_N \end{bmatrix}\begin{bmatrix} w_{11} & \cdots & w_{1N} \\ \vdots & \ddots & \vdots \\ w_{N1} & \cdots & w_{NN} \end{bmatrix}^{\mathrm{T}} = \tilde{\mathbf{Z}}\mathbf{\Gamma}\mathbf{W}^{\mathrm{T}}. \tag{3}$$

The decays have a straightforward relationship to the photokinetic matrix; they are products of the fundamental matrix, $\mathbf{W}$ (columns equal to the eigenvectors of $\mathbf{K}$), the initial condition matrix, $\mathbf{\Gamma}$, and fundamental, monoexponential decays, $\tilde{\mathbf{Z}}$ (decay rates equal to the eigenvalues of $\mathbf{K}$).

The Fourier transform of a derivative is linearly related to the Fourier transform of the original function. Consequently, the photokinetic transfer matrix, $\mathbf{K}$, is a linear function of the pure FT decays of the mixture components, $\tilde{\mathbf{Y}}$, and can be determined by solving the following system of linear equations

$$\tilde{\mathbf{Y}}^{\mathrm{T}}\tilde{\Omega} - \mathbf{Y}_0^{\mathrm{T}} = \mathbf{K}\tilde{\mathbf{Y}}^{\mathrm{T}} \tag{4}$$

where $\tilde{\Omega}$ is a diagonal matrix of complex excitation modulation frequencies and each row of $\mathbf{Y}_0$ is the initial concentration vector $\mathbf{y}_0$.[59] Solving the complex part of eq 4 yields the photokinetic matrix:

$$\mathbf{K} = (\tilde{\mathbf{Y}}^{\mathrm{T}}\tilde{\Omega})_{\mathrm{imag}}(\tilde{\mathbf{Y}}_{\mathrm{imag}}^{\mathrm{T}})^{+} \tag{5}$$

where the subscript "imag" refers to the imaginary part of the matrix and superscript $+$ denotes the pseudoinverse.[62] In addition to providing a nonheuristic estimate of $\mathbf{K}$, this approach also provides an estimate of the initial intensities, $\mathbf{Y}_0$, via rearrangement of eq 4.

Data Analysis. *Component Resolution*. Self-modeling curve resolution (SMCR)[63] is one approach to partitioning the data matrix, $\tilde{\mathbf{D}}$, into pure component spectra and decays, $\mathbf{X}$ and $\tilde{\mathbf{Y}}$. The central idea is to use the mathematical constraints on the spectra and decays, e.g., nonnegativity, to direct the transformation of orthogonal basis vectors of the matrix into physically relevant component responses. The principal components are mutually orthogonal basis vectors that capture the maximum matrix variance in the fewest vectors. The principal components also are linear combinations of the component spectra from

which each column of the matrix can be reconstructed. The principal components analysis (PCA) of $\tilde{\mathbf{D}}$ is

$$\tilde{\mathbf{D}} = \mathbf{X}\tilde{\mathbf{Y}}^{\mathrm{T}} = \mathbf{U}_{\tilde{\mathbf{D}}}\mathbf{B}_{\tilde{\mathbf{D}}}{}^{\mathrm{T}} \tag{6}$$

where $\mathbf{U}_{\tilde{\mathbf{D}}}$ is the matrix of principal components and $\mathbf{B}_{\tilde{\mathbf{D}}}$ is a matrix of principal component vector loadings. The loadings are coefficients that describe the expansion of each matrix column in terms of the principal components. Only N of the principal components describe the variance associated with the spectral signal. The remaining vectors describe noise and should be eliminated from the matrices $\mathbf{U}_{\tilde{\mathbf{D}}}$ and $\mathbf{B}_{\tilde{\mathbf{D}}}$ before further analysis. The component spectra, $\mathbf{X}$, and component decays, $\tilde{\mathbf{Y}}$, can be reconstructed from truncated matrices $\mathbf{U}_{\tilde{\mathbf{D}}}$ and $\mathbf{B}_{\tilde{\mathbf{D}}}$ by linear transformation. The transformation matrix, $\tilde{\mathbf{I}}\tilde{\mathbf{I}}$, that converts the column basis vectors, $\mathbf{U}_{\tilde{\mathbf{D}}}$, to spectra has an inverse that converts the loadings matrix, $\mathbf{B}_{\tilde{\mathbf{D}}}$, to FT decays, i.e.,

$$\mathbf{X} = \mathbf{U}\tilde{\mathbf{I}}\tilde{\mathbf{I}} \tag{7}$$

$$\tilde{\mathbf{Y}} = \mathbf{B}\tilde{\mathbf{I}}\tilde{\mathbf{I}}^{-\mathrm{T}} \tag{8}$$

The elements of $\tilde{\mathbf{I}}\tilde{\mathbf{I}}$ can be determined by minimizing physically impossible values in the component responses, e.g., negative or imaginary spectral profile values ($\mathbf{U}\tilde{\mathbf{I}}\tilde{\mathbf{I}}$), negative or imaginary initial intensities ($\mathbf{Y}_0$), nonnegative decay values (diagonal elements of $\mathbf{K}$), etc. If the decay constants of the components are moderately different and the spectra are not strongly overlapped, these constraints are sufficient to resolve the spectra and FT-decays from $\tilde{\mathbf{D}}$ with little ambiguity.[58]

Results and Discussion

Previous studies of PRODAN and LAURDAN indicate that the molecules exhibit different degrees of mobility and average position within membrane bilayers.[23,24,64] LAURDAN is anchored to the acyl chain core of membrane bilayers by a fatty acid tail. It is considered to be more deeply embedded in the membrane bilayer than PRODAN and is not considered to undergo changes in bilayer depth or fatty acid chain orientation during membrane phase transitions. The spectral shift in LAURDAN has been attributed to lipid and water molecule distribution around the probe.[25,47,64] PRODAN is considered to be much more mobile in membrane bilayers and to occupy a region (or several distinct regions) close to the lipid headgroup/water interface.[23,24] Considering these differences, one of the most interesting observations generated by multivariate analysis of the FT-EDMs of PRODAN and LAURDAN is the similarity of their emission properties. The FT-EDMs of PRODAN and LAURDAN were recorded as a function of temperature in DMPC vesicles, around the gel to liquid-crystal phase transition. Principal components analysis of PRODAN and LAURDAN FT-EDMs indicates remarkable similarity in the orthogonal components of the probes' emission. The principal components of PRODAN and LAURDAN at a given temperature were nearly identical (data not shown). The most significant difference between the principal components of the probes occurs near 520 nm, which is the emission maximum of PRODAN molecules in water.[65] PRODAN is moderately soluble in water and exhibits a low intensity emission in this region, whereas LAURDAN, which is confined to the bilayer region shows no such emission. It is also interesting that the rank analysis of the FT-EDMs of both probes indicates they consist of three independent components in most cases. As Figure 2 shows, it is clear that the first three principal components are substantially larger and contain much more low frequency information than

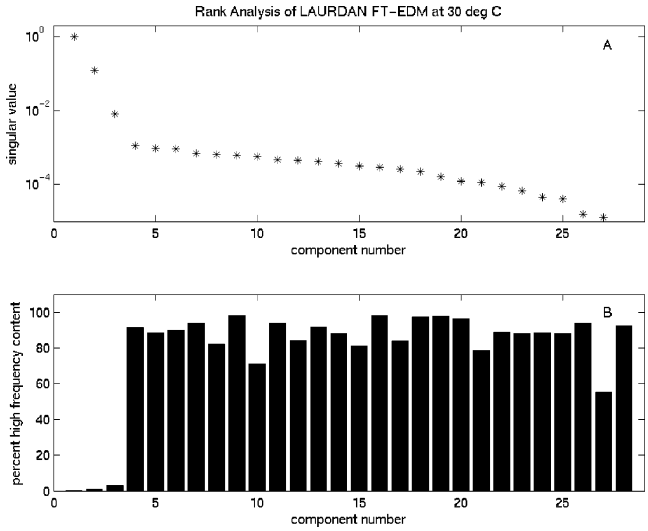

Figure 2. Rank analysis of a LAURDAN FT-EDM. (A) The logarithmic plot of eigenvalues obtained via principal components analysis of a LAURDAN data set measured at 30 °C. (B) The frequency content of the basis vectors. Lower frequency content corresponds to spectral response, higher frequency content is associated with random noise. These results were typical for all data, for both probes at or above the phase transition temperature.

the rest. These three capture the variance associated with probe response, whereas the other principal components describe the noise variance. This is typical for both probes, at all temperatures, with the notable exception of the PRODAN FT-EDMs at temperatures below the phase transition, which appear to consist of two independent components. The apparent differences in the emission of the probes are less significant when viewed in terms of the emission components. At temperatures below the phase transition, the steady state emission profile of PRODAN has a blue shifted maximum in comparison to LAURDAN. At temperatures much higher than the phase transition temperature, the PRODAN emission profile maximum is red shifted relative to that of LAURDAN. These observations are easily interpreted as evidence of the higher degree of mobility for PRODAN molecules within the membrane bilayer, but relative intensity data presented below indicate that they reflect the smaller contribution of the emission component at the center of spectrum in PRODAN.

The component spectra and decays of PRODAN and LAURDAN subpopulations in vesicles were resolved from FT-EDMs using PCA/SMCR. The photokinetic properties of the probes were estimated from FT-decays algebraically (see eq 5). In the case of LAURDAN, three spectrally distinct decay species were recovered at all temperatures studied. Modifying the assignments of Paternostre and co-workers, we label the blue-shifted species ($\lambda_{\max} \sim 415$ nm) locally excited (LE), the intermediate species ($\lambda_{\max} \sim 450$ nm) charge transfer (CT), and the most red-shifted species ($\lambda_{\max} \sim 490$ nm) solvent relaxed (SR) (see Figure 3A−C).[52,53] The resolved spectrum of the locally excited state compares favorably with the spectrum they recorded instantaneously ($t \sim 0$ ns) for LAURDAN incorporated in gel-phase DPPC vesicles.[54] At later acquisition times, their LAURDAN spectrum in gel phase DPPC vesicles was red-shifted and similar to what we recover for the charge transfer state. Three distinct spectral species were also resolved from PRODAN emission at most temperatures. However, the solvent-relaxed emission could not be recovered from the data at the lowest temperature recorded (20 °C). Also, the low intensity emission from PRODAN molecules in water (emission $\lambda_{\max} \sim$ 520 nm, see Figure 3A) could not be separated from the locally

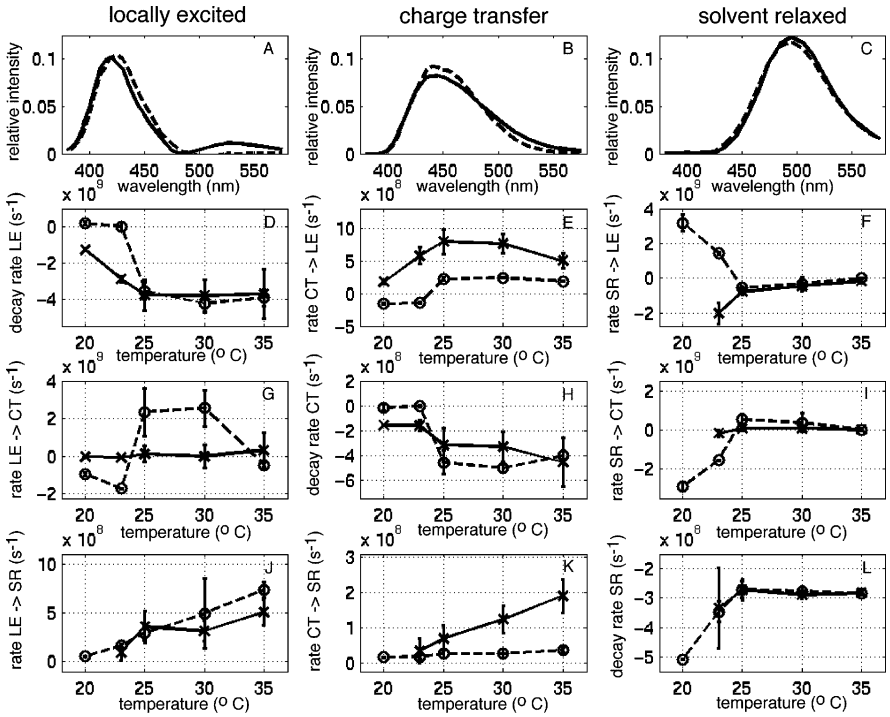

Figure 3. Resolved component spectra and photokinetics of PRODAN and LAURDAN. The component spectra of each emitting state (locally excited − LE, charge transfer − CT, solvent relaxed − SR) are displayed across the top of the figure (A−C) for PRODAN (solid lines) and LAURDAN (dashed lines). The kinetic data are presented in the form of the photokinetic transfer matrix (see Data Analysis section for details) as a function of temperature. The decay rates lie on the diagonal (D, H, L), and the off-diagonals correspond to the rates of association and dissociation between emitting states. The direction of transfer is labeled on the *y*-axis. PRODAN is designated by solid lines and x marks, LAURDAN by dashed lines and open circles. Note: To highlight changes in kinetics as a function of temperature, the magnitude of the *y*-axis varies for each decay/transfer rate plot. Error bars represent 95% confidence intervals.

excited state spectrum. Substantial temporal overlap made these two emitting species inseparable using PCA/SMCR. The maxima of the locally excited and solvent relaxed species of both probes were nearly constant as a function of temperature. The maxima and shape of the charge transfer species for both probes shifted slightly as a function of temperature (data not shown).

A comparison of the decay kinetics for PRODAN and LAURDAN is provided in Figure 3. The data are presented in the format of the photokinetic transfer matrix (described in eq 2) as a function of temperature augmented by the spectral profiles of each state in the top row (Figure 3A−C). The decay rates of each state are displayed along the diagonal (Figure 3D, H, and L). The decay rates of the locally excited states show the greatest variation between PRODAN and LAURDAN, especially at low temperatures. However, it should be noted that the decay times for the locally excited state were difficult to measure and appear to decay remarkably slowly. The decay rates of the charge transfer states of the two probes are similar, with LAURDAN exhibiting a slightly larger variation around the phase transition temperature (23 °C). The decay rates of the solvent-relaxed states of the two probes are nearly identical. The rates of conversion or transfer between emitting states are depicted on the matrix off-diagonals (Figure 3E−G, and 3I−K). The overall trends of these rates as a function of temperature are similar for the two probes. The analysis indicates that both the locally excited and charge transfer states are increasingly converted to solvent-relaxed species with temperature. However, the locally excited conversion rates are somewhat larger than the charge transfer conversion rates, especially in the case of LAURDAN. The analysis also indicates that the charge transfer species of PRODAN undergoes back conversion to the locally excited state. This apparent reversal is likely evidence of the impact of PRODAN mobility and membrane solubilization equilibria on the probe emission. Consequently, it is possible that the conversion of PRODAN charge transfer species to the solvent-relaxed state is similarly a reflection of membrane dynamics.

The initial and steady-state intensities of each state of PRODAN and LAURDAN as a function of temperature are depicted in Figure 4A−D. The initial intensity of the solvent relaxed state of each probe is negligible within experimental error at all temperatures. This is very clear evidence that the excited solvent relaxed species are not photoexcited, but formed by excited state processes. The initial and steady-state intensities reveal an interesting difference between the two probes. The intensities of the charge transfer component are much larger in LAURDAN than in PRODAN, whereas the intensities of the other species are comparable in both probes, a small difference in the locally excited intensity at and below the gel phase transition temperature notwithstanding.

Principal components analysis and self-modeling curve resolution impose minimal model assumptions on the decay analyses, but the assumption that the probe photokinetics are first order is inherent in the analysis. One way to evaluate the validity of this assumption is to investigate the nature of the fundamental, putatively monoexponential decays, $\tilde{\mathbf{Z}}$, underlying the component decays (see eq 3). Since the FT-EDM is a product of spectral and temporal factors, the fundamental decays are paired with spectral domain counterparts which have been called the decay-associated spectra (DAS).[66] The DAS are products of the component spectra and the fundamental matrix constructed from the eigenvectors of the photokinetic matrix (**X** and **W** in eqs 1 and 3). In other words, the decay-associated spectra are the linear combinations of the pure component spectra that decay as monoexponentials in a first order data

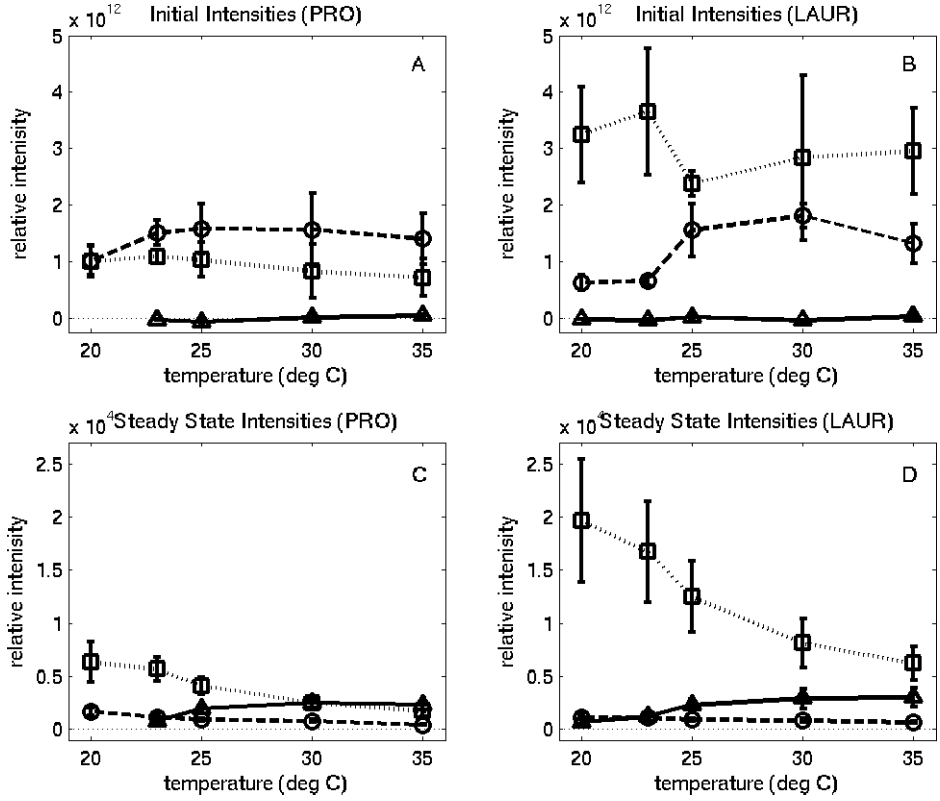

Figure 4. Initial intensities and steady-state intensity contributions for PRODAN and LAURDAN. The initial intensities and steady-state intensity contributions for PRODAN (A and C, respectively) and LAURDAN (B and D, respectively) are presented as a function of temperature. The emission states for both probes are denoted as follows: locally-excited (open circle, dashed line), charge-transfer (square, dotted line), solvent-relaxed (triangle, solid line). Error bars represent 95% confidence intervals.

matrix. Figure 5A depicts the decay-associated spectra recovered from the emission of LAURDAN in DMPC at 30 °C. Negative bands in the decay-associated spectra indicate that excited-state processes link the species contributing to the spectra,[67] because they mean that neither the fundamental matrix nor the photokinetic matrix are diagonal. (This is analogous to the recovery of negative pre-exponential factors in global or maximum entropy analysis.) The decay-associated spectra recovered from the FT-EDMs of LAURDAN in DMPC vesicles exhibit three main bands with maxima at ∼415 nm, ∼435 nm, and ∼490 nm. The first component (dashed lines) is dominated by emission from the solvent-relaxed state. The second component (dot−dashed lines) is a combination of all three components. The third component (solid lines) indicates interaction between the locally excited and solvent relaxed states. This decay-associated spectrum and the positive transfer rates (Figure 3J) indicate an excited state interaction between the locally excited and solvent relaxed states. However, the fundamental decay associated with this spectrum does not exhibit monoexponential decay kinetics. This is the case for both probes at all temperatures. Figure 5B is the Argand diagram of the fundamental decays of the data matrix collected from LAURDAN in DMPC at 30 °C. The first and second components (dominated by the charge transfer and solvent relaxed states) exhibit first order, monoexponential decay kinetics, as expected. The third component, which is dominated by the locally excited state, deviates substantially from this behavior, as evidenced by its deviation from the reference semicircle. A systematic deviation from a constant value is also observed in the initial intensity estimates of the locally excited state of both probes as a function of frequency at all temperatures (data not shown). Together these observations indicate deviation from first order kinetics which may be caused by a rank deficiency or a distortion in the decay due to measurement error. In the case of a rank deficiency, one, or more, decay process(es) associated with the recovered spectrum is (are) not properly accounted for. This could be due to unresolved spectral components in the decay-associated spectrum or the presence of decay processes that are not linked to unique spectra. Measurement error could be the result of the fast decay rate of the decay-associated species dominated by the locally excited species. In practical terms, the limited range of the modulation frequencies generated by our instrumentation applies a long-pass filter to the kinetics that may distort the decays of short-lived species disproportionately. Moreover, inadequate reference lifetime correction could introduce a systematic distortion to a very fast decay. The low intensities of this component and larger noise observed at higher modulation frequencies also can undermine the accuracy of the recovered decay kinetics. Preliminary analysis of frequency domain emission data acquired in the presence of an energy transfer acceptor and time domain data acquired using a faster detection system suggests that the locally excited band recovered here is a mixture of unresolved bands. This deviation from monoexponential behavior impacts the calculations of the rates presented in Figure 3 and likely contributes to the large error bars in the decay rate of the locally excited state as well as the rate of transfer from the locally excited to charge transfer state.

These PCA/SMCR results provide a view of the excited state processes of PRODAN and LAURDAN in lipid vesicles that, while still incomplete, contributes new elements to the photokinetic model for PRODAN and LAURDAN in lipid membranes. It is clear that at least three species contribute to the emission of these probes. The nonzero initial intensities recovered for two of these species support the existence of at least two excitation transitions, which are followed by a number of excited-state interactions. Paternostre and co-workers came

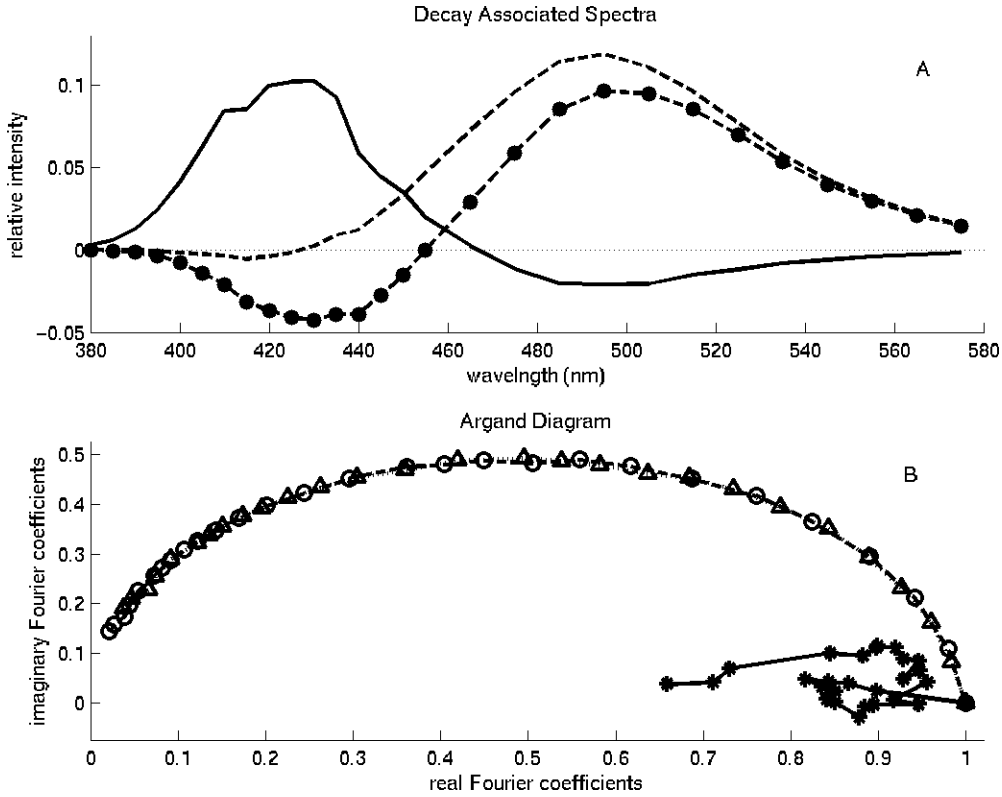

Figure 5. Decay associated spectra and fundamental decays of LAURDAN in DMPC at 30 °C. (A) Decay associated spectra. The first component (dashed line) is dominated by the solvent relaxed state emission. The second component (dot−dashed line) is dominated by the charge transfer and solvent relaxed states. The third component (solid line) is dominated by the locally excited state. Negative spectral contributions indicate excited state interactions between the components. (B) Argand diagram of fundamental decays. The first (dashed line, open circles) and second components (dotted line, triangles), dominated by the charge transfer and solvent relaxed states, follow monoexponential decay kinetics. The third component (solid line, * marks), dominated by the locally excited state, deviates from monoexponential behavior. This data set was typical for both probes at all temperatures above the phase transition.

to similar conclusions when observing excitation wavelength induced change in emission profile of LAURDAN in frozen ethanol (−190 °C) and viscous apolar oils at low temperatures, where solvent relaxation processes do not take place. They concluded that under these conditions the behavior of LAURDAN is consistent with a model proposed by Rollinson and Drickamer in which two excited states, the locally excited and charge transfer, originate from heterogeneity in absorption transitions: $\pi \rightarrow \pi^*$ and $n \rightarrow \pi^*$, respectively.[68] In the same study, Paternostre and co-workers observed two emission bands separated by an isoemissive point at higher temperatures (−110 °C to −50 °C), where solvent relaxation is expected. This led them to conclude that, on average, two principal excited states, which they labeled charge transfer and charge transfer solvent relaxed, are interconverting in this temperature range. Our results indicate that the solvent-relaxed species is not photoexcited and interconversion of the locally excited to the solvent relaxed state is the dominant transition of the two (See Figure 3J, K). In fact, the lack of charge transfer conversion in LAURDAN and the potential for contributions from probe/membrane dynamics to the PRODAN results suggest that there may be no direct interaction between the charge-transfer and solvent-relaxed species. Finally, our results show no evidence of the dynamic Stokes' shifts observed in conventional solvent relaxation.

Conclusions

We have investigated the fluorescence decay kinetics of PRODAN and LAURDAN in DMPC vesicles using multivariate statistical methods. The utility of multivariate analysis lies in taking advantage of the changes in decay profiles and spectral shifts simultaneously in order to collect the maximum amount of information about a system. One can recover information about individual excited states and their response to local environments in spite of spectral overlap. Although these probes are viewed as occupants of different positions within the membrane bilayer, their decay kinetics are remarkably similar. The recovered component spectra also are similar, with varying amounts of individual components producing the overall difference in the steady state profiles of the probes. These recovered component spectra are consistent with TRES of LAURDAN in the literature. Therefore, emission band assignments used here are modified from the three emissive state model proposed by Paternostre and co-workers. As they did, we see clear evidence for at least three emissive states with excited state interactions between them. Additionally, we observed evidence that two species are photoexcited, followed by post-excitation processes that generate the third emission component. However, the kinetic results differ substantially from their view. The species we call solvent relaxed is a product of the charge transfer species in the Paternostre model, but generated from the locally excited species in our multivariate analysis. Moreover, we do not see evidence of conventional solvent relaxation in this emission component. Little change in the spectral band position, shape, or decay kinetics was observed in any of the three species as a function of temperature. Combining the multivariate analysis results with the implications of the work in protic solvents reported in the literature, we speculate that the solvent relaxed species is hydrogen bonded. It is clear that hydrogen bonding alone does not account for the dramatic shift from ∼415 nm to ∼490 nm, but geometric and/or electronic changes coupled to

hydrogen bonding may account for this observation. In any case, the presence of at least three emissive states at temperatures above and below the phase transition argues against the widely held notion of two phase-dependent components in lipid membranes.

The work presented here was motivated by the challenges in characterizing lipid membranes with sufficient selectivity to measure variations around bulk properties. A more extensive investigation of the nature of the states underlying PRODAN and LAURDAN emission is required to resolve the details needed to achieve this goal. However, the comparison of the probes' emission revealed differences that raise interesting questions about the nature of the emitting states. It is remarkable that the most significant differences between the photokinetics of the two probes involve the species labeled charge transfer. The differences in the conversion rates of this species in the two probes are interesting, but the ambiguity regarding the source of this difference (lipid dynamics vs photokinetics) makes these data difficult to interpret. On the other hand, it is clear that this species is much more prominent in the LAURDAN emission than that of PRODAN, while the other components have comparable emission intensities in the two probes. This observation is difficult to rationalize on the basis of a more polar PRODAN solubilization site. Nor is it consistent with the expectation that charge transfer would be larger in the case of PRODAN, which is more mobile and thus has access to more flexible lipid environment in the bilayer. On the other hand, these results are consistent with the idea that the hydration of the bilayer plays a significant role in the probes' photokinetics. If future work confirms this result, this dependence can be exploited to distinguish membrane hydration and lipid phase, increasing the selectivity of probe PRODAN and LAURDAN emission measurements of membrane processes.

Acknowledgment. This work is supported by the National Science Foundation (Grant CHE-9983558).

References and Notes

(1) Kimelberg, H. K. *Cell Surf. Rev.* **1977**, *3*, 205.
(2) Conforti, G.; Zanetti, A.; Paquali-Ronchetti, I.; Quaglino, D.; Neyroz, P.; Dejana, E. *J. Biol. Chem.* **1990**, *265*, 4011.
(3) Kuo, P.; Weinfeld, M.; Loscalzo, J. *Biochemistry* **1990**, *29*, 6626.
(4) Sherbet, G. V. *Exp. Cell Biol.* **1989**, *57*, 198.
(5) Klausner, R. D.; Kleinfeld, A. M.; Hoover, R. L.; Karnovsky, M. J. *J. Biol. Chem.* **1980**, *255*, 1286.
(6) Lentz, B. R.; Clubb, K. W.; Alford, D. R.; Hochi, M.; Meissner, G. *Biochemistry* **1985**, *24*, 433.
(7) Klymchenko, A. S.; Demchenko, A. P. *Langmuir* **2002**, *18*, 5637.
(8) Klymchenko, A. S.; Duportail, G.; Ozturk, T.; Pivovarenko, V. G.; Mely, Y.; Demchenko, A. P. *Chem. Biol.* **2002**, *9*, 1199.
(9) Klymchenko, A. S.; Ozturk, T.; Demchenko, A. P. *Tetrahedron Lett.* **2002**, *43*, 7079.
(10) Ercelen, S.; Klymchenko, A. S.; Demchenko, A. P. *Anal. Chim. Acta* **2002**, *464*, 273.
(11) Sytnik, A.; Litvinyuk, I. *Proc. Natl. Acad. Sci. U.S.A.* **1996**, *93*, 12959.
(12) Weber, G.; Farris, F. J. *Biochemistry* **1979**, *18*, 3075.
(13) Massey, J. B.; She, H. S.; Pownall, H. J. *Biochemistry* **1985**, *24*, 6973.
(14) Sommer, A.; Paltauf, F.; Hermetter, A. *Biochemistry* **1990**, *29*, 11134.
(15) Rottenberg, H. *Biochemistry* **1992**, *31*, 9473.
(16) Bondar, O. P.; Rowe, E. S. *Biophys. J.* **1999**, *76*, 956.
(17) Krasnowska, E. K.; Bagatolli, L. A.; Gratton, E.; Parasassi, T. *Biochim. Biophys. Acta* **2001**, *1511*, 330.
(18) Sengumpta, B.; Guharay, J.; Sengumpta, P. K. *Spectrochim. Acta, Part A* **2000**, *56*, 1433.
(19) Bernik, D. L.; Zubiri, D.; Tymczyszyn, E.; Disalvo, E. A. *Langmuir* **2001**, *17*, 6438.
(20) Hutterer, R.; Hof, M. *J. Fluoresc.* **2001**, *11*, 227.
(21) Bondar, O. P.; Rowe, E. S. *Biophys. J.* **1996**, *71*, 1440.
(22) Parasassi, T.; Giusti, A. M.; Gratton, E.; Monoco, E.; Raimondi, M.; Ravagnan, G.; Sapora, O. *Int. J. Radiat. Biol.* **1994**, *65*, 329.
(23) Chong, P. L.-G. *Biochemistry* **1988**, *27*, 399.
(24) Chong, P. L.-G.; Zeng, J. *Biochemistry* **1991**, *30*, 9485.
(25) Parasassi, T.; Krasnowska, E. K.; Bagatolli, L. A.; Gratton, E. *J. Fluoresc.* **1998**, *8*, 365.
(26) Lakowicz, J. R.; Balter, A. *Biophys. Chem.* **1982**, *16*, 117.
(27) Chapman, C. F.; Fee, R. S.; Maroncelli, M. *J. Phys. Chem.* **1990**, *94*, 4929.
(28) Chapman, C. F.; Maroncelli, M. *J. Phys. Chem.* **1991**, *95*, 9095.
(29) Lobo, B. C.; Abelt, C. J. *J. Phys. Chem.* A **2003**, *107*, 10938.
(30) Davis, B. N.; Abelt, C. J. *J. Phys. Chem.* A **2005**, *109*, 1295.
(31) Nowak, W.; Adamczak, P.; Balter, A.; Sygula, A. *J. Molec. Struct. (THEOCHEM)* **1986**, *139*, 13.
(32) Ilich, P.; Prendergast, F. G. *J. Phys. Chem.* **1989**, *93*, 4441.
(33) Parusel, A. B. J.; Schneider, F. W.; Kohler, G. *Theochem.−J. Molecul. Struct.* **1997**, *398*, 341.
(34) Parusel, A. B. J. *J. Chem. Soc., Faraday Trans.* **1998**, *94*, 2923.
(35) Parusel, A. B. J.; Nowak, W.; Grimme, S.; Kohler, G. *J. Phys. Chem. A* **1998**, *102*, 7149.
(36) Heisel, F.; Miehe, J. A.; Szemik, A. W. *Chem. Phys. Lett.* **1987**, *138*, 321.
(37) Bunker, C. E.; Bowen, T. L.; Sun, Y.-P. *Photochem. Photobiol.* **1993**, *58*, 499.
(38) Balter, A.; Nowak, W.; Pawelkiewicz, W.; Kowalczyk, A. *Chem. Phys. Lett.* **1988**, *143*, 565.
(39) Catalan, J.; Perez, P.; Laynez, J.; Blanco, F. G. *J. Fluoresc.* **1991**, *1*, 215.
(40) Zurawsky, W.; Scarlata, S. *J. Phys. Chem.* **1992**, *96*, 6012.
(41) Samanta, A.; Fessenden, R. *J. Phys. Chem. A* **2000**, *104*, 8972.
(42) Nyholm, T.; Nylund, M.; Soderholm, A.; Slotte, J. P. *Biophys. J.* **2003**, *84*, 987.
(43) Hutterer, R.; Schneider, F. W.; Sprinz, H.; Hof, M. *Biophys. Chem.* **1996**, *61*, 151.
(44) Hutterer, R.; Parusel, A. B. J.; Hof, M. *J. Fluoresc.* **1998**, *8*, 389.
(45) Krasnowska, E. K.; Gratton, E.; Parasassi, T. *Biophys. J.* **1998**, *74*, 1984.
(46) Parasassi, T.; De Stasio, G.; d'Ubaldo, A.; Gratton, E. *Biophys. J.* **1990**, *57*, 1179.
(47) Parasassi, T.; De Stasio, G.; Ravagnan, G.; Rusch, R. M.; Gratton, E. *Biophys. J.* **1991**, *60*, 179.
(48) Parasassi, T.; Ravagnan, G.; Rusch, R. M.; Gratton, E. *Photochem. Photobiol.* **1993**, *57*, 403.
(49) Parasassi, T.; Loiero, M.; Raimondi, M.; Ravagnan, G.; Gratton, E. *Biochim. Biophys. Acta* **1993**, *1153*, 143.
(50) Parasassi, T.; DiStephano, M.; Loiero, M.; Ravagnan, G.; Gratton, E. *Biophysical J.* **1994**, *66*, 763.
(51) Bagatolli, L. A.; Maggio, B.; Aguilar, F.; Sotomayor, C. P.; Fidelio, G. D. *Biochim. Biophys. Acta* **1997**, *1325*, 80.
(52) Bagatolli, L. A.; Parasassi, T.; Fidelio, G. D.; Gratton, E. *Photochem. Photobiol.* **1999**, *70*, 557.
(53) Gratton, E.; Limkeman, M.; Lakowicz, J. R.; Laczko, G.; Cherek, H. *Biophys. J.* **1984**, *46*, 463.
(54) Viard, M.; Gallay, J.; Vincent, M.; Paternostre, M. *Biophys. J.* **2001**, *80*, 347.
(55) Viard, M.; Gallay, J.; Vincent, M.; Meyer, O.; Robert, B.; Paternostre, M. *Biophys. J.* **1997**, *73*, 2221.
(56) Vanounou, S.; Pines, D.; Pines, E.; Parola, A. H.; Fishov, I. *Photochem. Photobiol.* **2002**, *76*, 1.
(57) Neal, S. L. *Anal. Chem.* **1997**, *69*, 5109.
(58) Villegas, M. M.; Neal, S. L. *J. Phys. Chem. A* **1997**, *101*, 6890.
(59) Neal, S. L. *J. Phys. Chem. A* **1997**, *101*, 6883.
(60) Wold, S. *Technometrics* **1978**, *20*, 397.
(61) Rossi, T. M.; Warner, I. M. *Anal. Chem.* **1986**, *58*, 810.
(62) Strang, G. *Linear Algebra and Its Applications*, 3rd ed.; Harcourt Brace Jovanovich Publishers: San Diego, 1988.
(63) Lawton, W. H.; Sylvestre, E. A. *Technometrics* **1971**, *13*, 617.
(64) Chong, P. L.-G.; Wong, P. T. T. *Biochim. Biophys. Acta* **1993**, *1149*, 260.
(65) Sun, S.; Heitz, M. P.; Perez, S. A.; Colon, L. A.; Bruckenstein, S.; Bright, F. V. *Appl. Spectrosc.* **1997**, *51*, 1316.
(66) Lofroth, J. E. *J. Phys. Chem.* **1986**, *90*, 1160.
(67) Lakowicz, J. R. *Principles of Fluorescence Spectroscopy*, 2nd ed.; Plenum Publishing Co.: New York, 1999.
(68) Rollinson, A. M.; Drickamer, H. G. *J. Chem. Phys.* **1980**, *73*, 5981.